Chapter 5

Cu(II) complex loaded triazine based porous organic polymer to promote benzylic C−H activation reactions

5.1 Abstract

The triazine based amide functional POP-Am2 discussed in Chapter 4 has been subjected for impregnation of Cu(II) ions on to transform the material into catalytic scaffold towards benzylic C–H activation reactions. Effective and efficient catalytic activity towards activation and oxidation of benzylic C–H in methylarenes to give benzaldehydes selectivity via benzyl alcohol as intermediate has been observed. A free radical reaction pathway via nucleophilic C–H activation has been proposed and demonstrated in this chapter.

5.2 Introduction

Selective functionalization of hydrocarbons through C–H bond activation affording oxidized products under environment friendly and mild reaction conditions is of concern from industrial perspectives [1-4]. Such activation was deliberated as unusual exemptions in the synthetic chemistry. However, in present days it becomes a vital thought while designing the synthetic reaction procedure and cannot be overlooked [5]. The C–H activation reaction provides opportunity for the formations of C−C and C−X (X = Heteroatom) bond following the various chemical processes involved in the reaction mechanism [6-17]. In general, palladium, the champion metal as catalyst has extensively used for the activation and functionalization of C–H bond [18-23]. But, the activity of other transition metals cannot be ignored. To mention a few, Ru(II)-diimine complex in recent days emerge as visible light photosensitizer in trifluoromethylation of arenes via C–H bond cleavage [24]. The carbonylation of C(sp^2)–H and N–H bond in amide has been demonstrated through cobalt catalyzed electrochemical oxidative process [25]. A scandium catalyzed C–C bond formation between methyl sulfides and unactivated alkenes is illustrated following regioselective α-C(sp^3)–H addition [26]. Limited examples of copper catalyzed C(sp^3)–S bond formation has also been reported during the sulfoxidation of benzylic C–H bond [27,28]. Notable achievements in the expansion of copper catalyst replacing the otherwise predominant and expensive Pd(II) catalyst in C–X bond formation [29-31] turned attention to functionalize C–H bond using

inexpensive Cu(II) catalyst. The C–H activation and functionalization reactions are also accomplished by metal organic frameworks (MOFs) or mixed metal catalysts. A Pd metallized zirconium (Zr) based MOF with thiocatechol in the architecture is demonstrated to oxidize regioselective sp^2 C–H bond. Presence of sulphur atom in the architecture of MOF with strong π-electron donating capability provides opportunity for immobilization of Pd on to MOF. Thereafter the active sites of metal get charged to accomplish oxidation of the aromatic C–H bond to give ethers and aryl halides respectively [32]. However, the organic transformation reactions are associated with electron push-pull mechanism. Hence, the enhancement or availability of π-electrons in the catalyst surface facilitates the reaction processes. In this perspective, POPs with continuous π-conjugation in its network remain advantageous than MOFs. The π-electrons or the lone pair electrons in the ligands used to synthesize MOFs is in coordination with the electropositive metal ions. Thus there prevails higher energy gap between the HOMO and LUMO in MOFs which reduces electronic transition and limiting the possibility of oxidation and reduction reactions. Inclusion of heteroatom such as N in the framework of POPs/COFs provides better opportunity with low band gap energy and higher electronic transition to act as metal-free catalyst or as catalytic bed for fine incorporation of metal catalysts. Organocatalyst provides newer road towards greener method reducing the toxic effect of metals. Sanzhong et al. while illustrating the functionalization of various C–H bond illustrates the catalytic activities of organic catalysts in this context [33].

Toluene, an aromatic hydrocarbon possessing sp^3 hybridized benzylic C–H bond can generate value-added oxidized products namely benzyl alcohol, benzaldehyde and benzoic acid [34]. Owing to its mammoth significance in our day-to-day life, benzaldehyde is the most anticipated product by the researchers and the most preferred and selective transformation reaction investigated and presented in this thesis [35]. Its utility ranges in the manufacturing industries of dyes, plasticizers, preservatives, organic solvents, perfumes, etc. It is also an important intermediate in pharmaceutical industries for the synthesis of drug molecules like chloramphenicol, ephidrin, analgin, etc. But benzaldehyde tends to over oxidize to give benzoic acid. Tuned reaction conditions and adding additives during the reaction process could improvise the benzaldehyde selectivity [36,37]. Thus the selective synthesis of benzaldehyde with good yield and stability is of highly desired. Customarily, it is produced from toluene by the chlorination

of methyl group to give dichloromethyl benzene as intermediate [38]. This intermediate subsequently undergoes saponification process to yield benzaldehyde. But, the product contains chlorinated impurities and not suitable to prescribe for food and drug industries. In addition, these processes cause environmental problems producing waste. Moreover these methods lack in efficiency. Antonietti group employed mesoporous carbon nitride doped with boron for the selective oxidation of toluene to benzaldehyde but with poor conversion yield [39, 40]. Graphene oxide acts as excellent solid support for incorporation of Pd nanoparticles in order to direct the activation of aromatic C–H bond [41].

Porous organic polymer (POP) with carboxyl functionality as carbocatalyst for the formation of C–C bond via C–H bond activation in indole is demonstrated [42]. Apart from catalysis porous polymers with high thermal and structural stabilities exhibits as versatile porous materials for adsorption and separation of gas molecules [43,44], in sensing [45,46], in conduction [47,48], etc. POPs rich in conjugated π-electrons propagated by carboxamide functionality acts as organic catalyst in selective oxidation of benzyl alcohols to benzaldehydes (refer to chapter 2) [49]. The π-electrons rich POP with N heteroatom provides platform for metals to coordinate. Similar behavior is reflected by pyridine ring based carboxamide POP demonstrated in Chapter 3 acting as heterogeneous catalyst carrier [50]. This Cu incorporated POP shows remarkable catalytic activity in reduction of 4-nitrophenol to 4-aminophenol than those displayed by other precious metal supported porous polymers. The nitrogen rich triazine ring based POP acting as organocatalyst in the C=C bond cleavage of α-aryl substituted olefins (refer to Chapter 4), a rare outcome in olefin oxidation with metal free catalyst is illustrated. The metal supported POPs exhibits remarkable activity as heterogeneous catalyst in biofuel production and in biorefinery [51]. Encouraged by such beautiful applications of POPs in organic transformation reactions, the π-electron rich triazine POP (POP-Am2) discussed in previous chapter is considered as scaffold to immobilize Cu(II) onto it (Scheme 5.1). The Cu impregnated POP-Am2 (Cu@POP-Am2 hereafter) reflects efficient and effective heterogeneous catalytic activity in activation and functionalization of unactivated benzylic sp^3 C–H bond of methylarenes (Table 5.1) to benzaldehydes with major selectivity and stability.

5.3 Results and discussion

5.3.1 Synthesis of Cu@POP-Am2

The POP-Am2 synthesized from nitrogen rich triazine based building block 2,4,6-tris(4-aminophenyl)triazine (TAPT) and trimesoyl chloride (BzCl) as linker was characterized utilizing FT-IR, ^{13}C CP-MAS NMR, PXRD, TGA, BET surface area analyzer, SEM and TEM analytical techniques. The detail explanations about the synthesis and characterization have been discussed in Chapter 4. Thus characterized POP-Am2 has been used as support matrix for immobilization of Cu(II) affording Cu@POP-Am2 (Scheme 5.1).

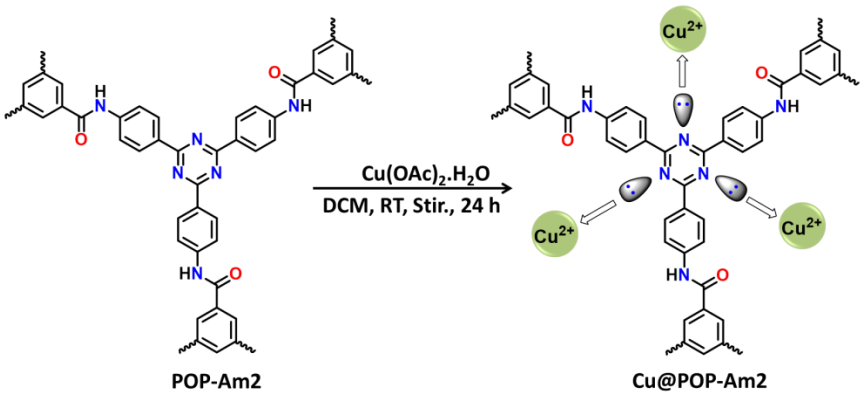

Scheme 5.1 (a) Synthetic representation of Cu immobilized POP-Am2, Cu@POP-Am2.

5.3.2 Characterization of Cu@POP-Am2

The desired Cu@POP-Am2 is characterized using FT-IR, PXRD, TGA, BET surface area analyzer, EDX, XPS and SEM analytical tools. To examine the change associated in the structural integrity of POP-Am2 after impregnation of copper, relevant spectral data obtained for Cu@POP-Am2 and compared with bare POP-Am2. Comparing the IR spectra of Cu@POP-Am2 with POP-Am2 (Figure 5.1a) depicts the preserved characteristic peaks for the stretching frequency of amide C=O at 1659 cm^{-1} and triazine ring at 1503 and 1360 cm^{-1} respectively. This established that upon docking the non-noble metal such as copper into the π-electron rich POP-Am2 support matrix the architecture of POP-Am2 was not altered.

From TGA analysis, it is validated that Cu@POP-Am2 shows thermal stability up to 400 °C (Figure 5.1b). The changes occurred, if any, in the structural integrity of bare POP-Am2 upon impregnation of copper was examined by recording the PXRD pattern of

Cu@POP-Am2. The overlaid pattern of Cu(II) loaded and bare POP-Am2 (Figure 5.2a) reveals the identical structural features with undisturbed integral stability of Cu@POP-Am2. Perhaps, the Cu(II) incorporated in the pore is finely dispersed and buried inside the pores of POP-Am2 and not sufficiently large sized Cu particle to diffract which is responsible for the presence of Cu(II).

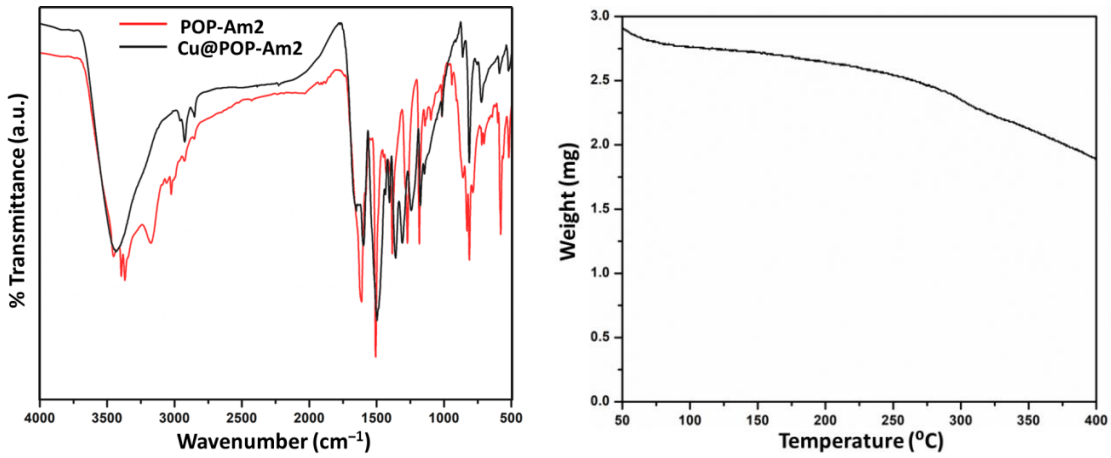

(a) (b)

Figure 5.1 (a) Comparison of IR spectrum of Cu@POP-Am2 and POP-Am2. (b) TGA plot exhibiting the thermal stability of Cu@POP-Am2 up to 400 ºC (b).

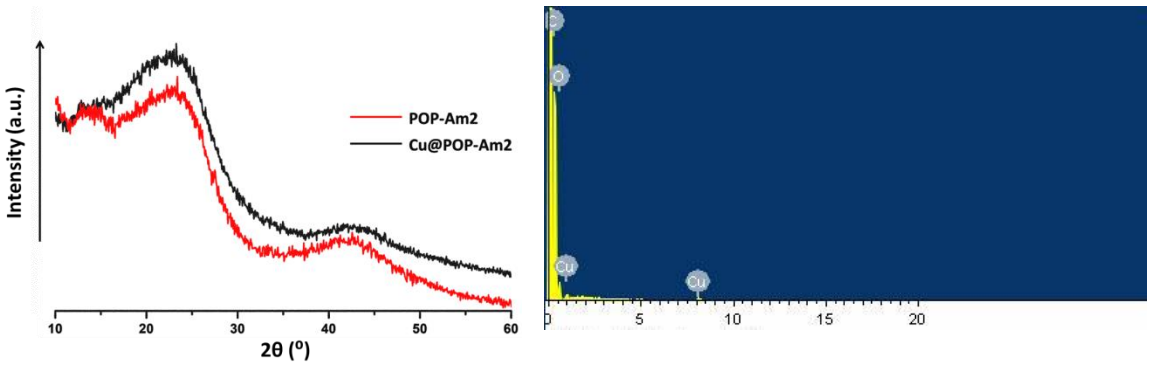

(a) (b)

Figure 5.2 (a) PXRD pattern of Cu@POP-Am2 laid over bare POP-Am2 reveals the perseverance of structural integrity of POP-Am2 upon loading with copper. (b) EDS spectrum confirms the existence of Cu in Cu@POP-Am2.

Moreover, the distribution of copper was further analyzed by recording the EDS spectrum of Cu@POP-Am2 (Figure 5.2b) and the amount of Cu loaded on POP-Am2 was calculated at 1.42 % by weight. The firm evidence about the interaction and oxidation state of Cu in Cu@POP-Am2 is obtained by performing XPS analysis and discussed later. The porosity and rigidity of bare POP-Am2 and copper salt impregnated

POP-Am2 i.e. Cu@POP-Am2 is analyzed by performing the nitrogen adsorption-desorption isotherm (Figure 5.3) and in both cases it was found to be type II adsorption isotherm. From the experiment the BET surface area and pore radius of POP-Am2 are calculated to be 51 m^2g^{-1} and 0.75 nm respectively (details in Chapter 4). The surface area and pore radius of Cu@POP-Am2 are found at 42 m^2g^{-1} and 1.8 nm respectively from BET isotherm. Lowering in surface area further confirms the incorporation of copper onto POP-Am2. Similarly increase in pore radius attributes the expansion of pore size due to localization of copper salt into the pores. The SEM images explain the surface morphology of Cu@POP-Am2. Figure 5.4a depicts the highly porous surface of POP-Am2. Upon incorporation of Cu, Cu@POP-Am2 displays the porous morphology with distribution and agglomeration of particles (Figure 5.4b).

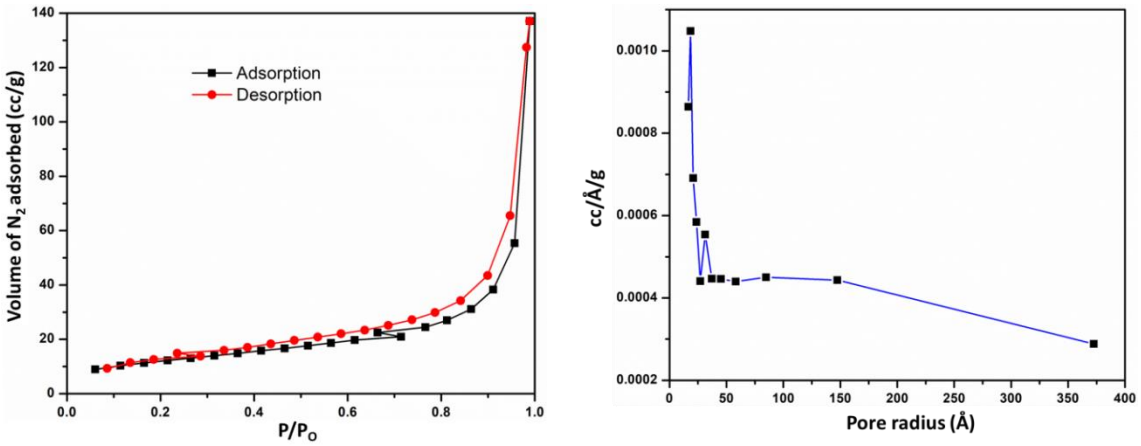

(a) (b)

Figure 5.3 Nitrogen adsorption-desorption isotherm (a) and pore size distribution curve (b) of Cu@POP-Am2.

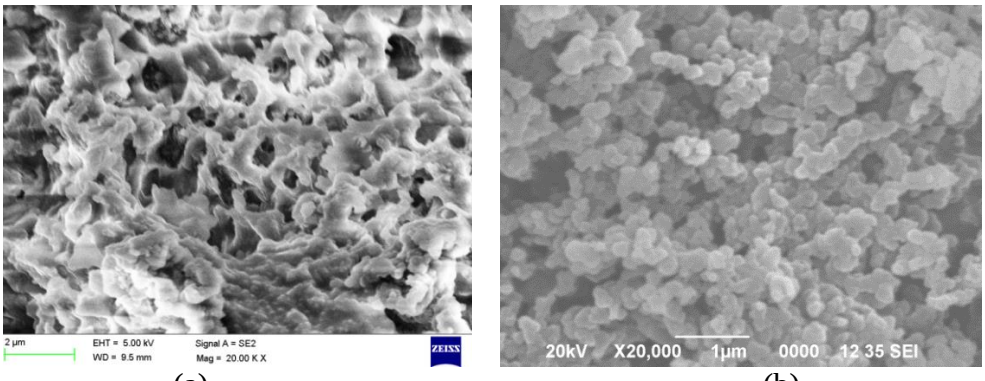

(a) (b)

Figure 5.4 FE-SEM image of POP-Am2 (a) and SEM image of Cu@POP-Am2 (b).

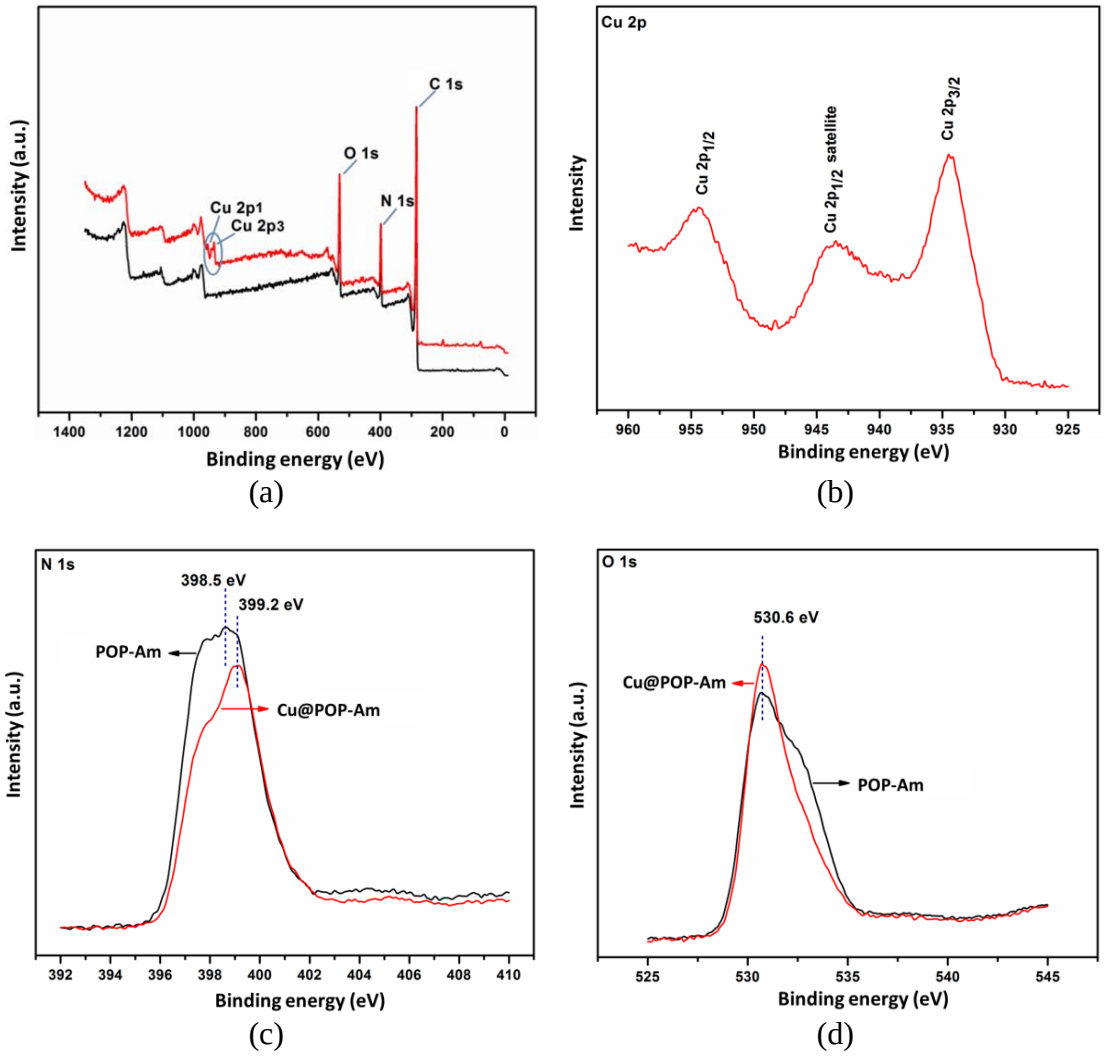

Figure 5.5 XPS spectra of (a) POP-Am2 (black) and Cu@POP-Am2 (red); (b) Cu 2p of Cu@POP-Am2; (c) N 1s and (d) O 1s spectra revealing the presence of Cu(II) and its interaction with N of POP-Am2.

For better understanding about the incorporation of copper salt into POP-Am2 and its interaction site the XPS analyses of bare POP-Am2 and Cu@POP-Am2 (Figure 5.5) were performed. Two unique signals (circled blue) in the XPS spectrum of Cu@POP-Am2 are responsible for Cu(II) clearly witnessed the incorporation of Cu (II) onto the π-electron rich POP-Am2. It is expected that incorporation of Cu(II) ion onto the POP-Am2 occurs via two available interaction sites i.e. N and O. The N 1s spectrum (Figure 5.5c) reveals the shifting of C–N signals from 398.5 eV in POP-Am2 to 399.2 eV in Cu@POP-Am2. This shifting in binding energy by 0.7 eV conferred the interaction of Cu(II) with the lone pair of N. However O 1s XPS spectrum (Figure 5.5d) depicts the band for C–O at 530.6 eV in POP-Am2 that remains undisturbed even after the incorporation of copper acetate. This observation confirms the fact that no interaction

takes place between the O-atom and Cu(II) ion. Moreover, the Cu 2p XPS spectrum (Figure 5.5b) depicted three bands at 934.5 eV, 943.5 eV and 954.3 eV. The two binding energies at 934.5 eV and 954.3 eV correspond to Cu $2p_{3/2}$ and Cu $2p_{1/2}$ respectively. However, a satellite peak appears at 943.5 eV due to complexation of Cu(II) with N lone pair in POP-Am2.

5.3.3 Oxidation of TEXM (T= toluene, E= ethyl benzene, X= xylene, M= mesitylene)

The electron density surrounding the copper in Cu@POP-Am2 enhances due to transfer of electrons from the π-electrons rich POP-Am2. Thereby, Cu@POP-Am2 acts as a nucleophile and facilitates activity towards nucleophilic organic transformation reactions. Thus the catalyst has been investigated for the oxidation of benzylic C–H in toluene with TBHP as the oxidant (Scheme 5.2). The progress of the reaction was initially monitored by TLC followed by recording GC-MS of the reaction mixture aliquot.

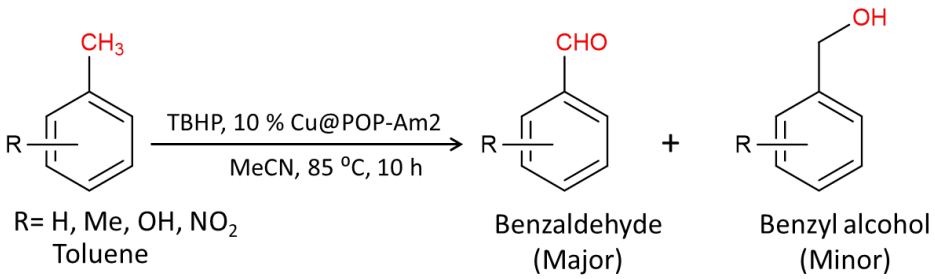

Scheme 5.2 Catalytic oxidation of benzylic C–H in toluene using Cu@POP-Am2 affording benzaldehyde with major selectivity.

In the process of finding optimized reaction parameters, temperature was found to have a prominent influence on oxidizing benzylic C–H of toluene. The catalytic reaction does not proceed at room temperature (RT) and the conversion increases sharply as the temperature raises. The maximum conversion of toluene with catalyst, Cu@POP-Am2 10 % (w/w) with respect to the toluene occurs at 85 °C and above. Eventually the conversion remains constant above 85 °C (Figure 5.6). Functionalization and oxidation of benzylic C–H is facilitated by the formation of benzyl alcohol as intermediate stabilized on the catalyst surface. With rise in temperature thus formed benzyl alcohol further gets oxidized to benzaldehydes and subsequently the benzaldehyde selectivity increases.

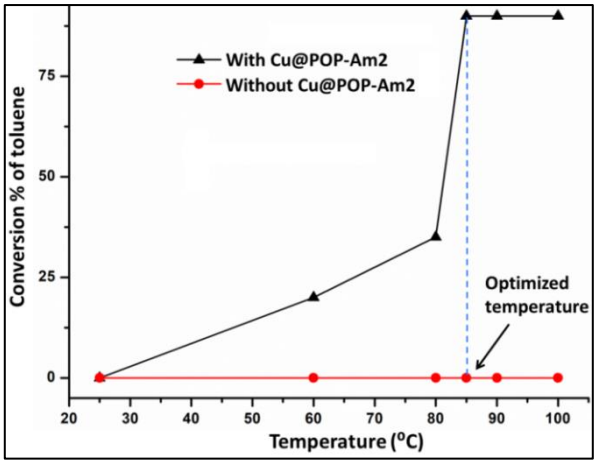

Figure 5.6 Temperature optimization vs conversion % in oxidation of toluene via sp^3 C–H activation.

Table 5.1 Cu@POP-Am2 catalyze activation and oxidation of benzylic C–H of TEXM

Entry	Reactant	TBHP (eq)	Conversion (%)	Product (%)	
1	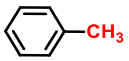	2	>90	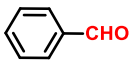 70	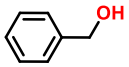 30
2	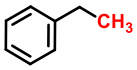	2	34	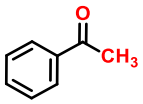 100	
3	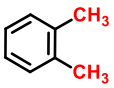	4	45	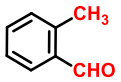 100	
4	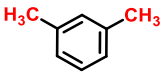	4	47	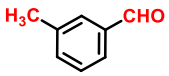 100	
5		6	17	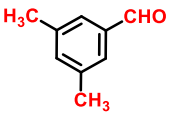 82	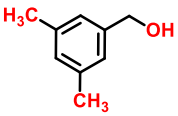 18
6	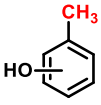	2	Nil	–	–
7	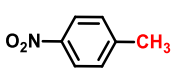	2	Nil	–	–

*Reaction conditions: toluene substrate (100 µL), MeCN (1 mL), reactions performed in schlenk tube and characterized using GC-MS.

The successful oxidative cleavage of benzylic sp^3 C–H bond in toluene with benzaldehyde selectivity prompted us to evaluate if Cu@POP-Am2 is equally effective for substituted toluene. The oxidation of methyl substituted toluene (Table 5.1) at the optimized conditions was subjected to examine product formation and confirmed by injecting the aliquot into GC-MS. Same reaction displayed in Table 5.1 was also carried out in presence of H_2O_2 as oxidant in lieu of TBHP. But the reaction progresses with negligible product yield (Table 5.2). As discussed in Chapter 2, it is possibly due to the strong leaching ability of H_2O_2. Moreover, its utility in non-polar and anhydrous solvent is restricted since it is not readily miscible. In addition, TBHP generates relatively stable and bulky radicals than H_2O_2 analogs. As a result the free diffusion of TBHP from the catalyst surface or pores is restricted allowing the catalytic reactions to occur smoothly.

Table 5.2 Oxidant screening in oxidation of benzylic C–H of TEXM

Entry	Oxidant	Conversion (%)
1	TBHP	> 90
	H_2O_2	Trace
2	TBHP	34
	H_2O_2	-
3	TBHP	45
	H_2O_2	Trace
4	TBHP	47
	H_2O_2	Trace
5	TBHP	17
	H_2O_2	-
6	TBHP	-
	H_2O_2	-
7	TBHP	-
	H_2O_2	-

It is observed that with the inclusion of methyl group in the benzene ring of toluene the conversion yield decreases gradually. As in the case of *o*- and *m*-xylene the conversion yield decreases to 47%. Mesitylene having three methyl groups experience only 17 % conversion under identical reaction conditions. In each of these methyl substituted

toluene only one methyl group is profound to oxidize with remaining methyl group being unaffected. It is because once a methyl group is oxidized to corresponding formyl group, the oxidation potential of the reactant further decreases due to the presence of electron withdrawing substituent. Thus the rate of oxidation process decreases. The Cu@POP-Am2 also oxidizes ethyl benzene to acetophenone. The isomeric cresol and nitro toluene were also examined while investigating the catalytic effect of Cu@POP-Am2 in benzylic C–H activation and oxidation. But no change in the reaction was observed. Same as formyl substituent, nitro group is also electron withdrawing substituent which decreases the oxidation potential of nitro toluene and the oxidation of methyl group is restricted. From the electronic environment in the catalyst and in hydrocarbon the reaction was expected to proceed through free radical mechanism. Accordingly the oxidation reaction of toluene with identical reaction conditions in Table 5.1 was tested in presence of TEMPO, a free radical scavenger (Scheme 5.3). As expected the reaction freezes suddenly proving its occurrence through free radical pathway.

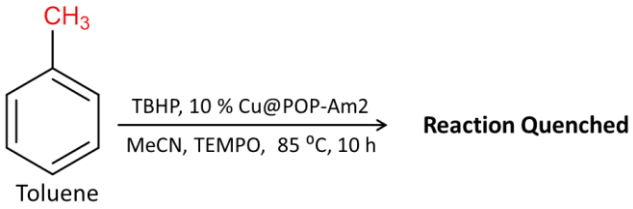

Scheme 5.3 Reaction quenching in catalytic oxidation of benzylic C–H in toluene using Cu@POP-Am2 in presence of TEMPO, a free radical scavenger.

5.3.4 Catalyst reusability test

To elucidate the reusability efficiency of Cu@POP-Am2, oxidation of toluene under identical reaction conditions as discussed in earlier Chapters as well as in the experimental section was performed. The conversion % in each cycle is depicted in figure 5.7. The catalyst after each cycle was recovered by centrifugation, washed thoroughly with acetone and methanol and vacuum dried before it is used for the subsequent cycle. The Cu@POP-Am2 catalyst is used up to three runs without obvious or much loss in the activity and conversion % of toluene. Thus the conversion of toluene remains constant for the first two cycles and it decreases thereafter. However, sudden decrease in the conversion % was observed at the fourth cycle.

In order to verify the leaching of copper during the catalytic process the hot filtration technique was employed. As the reaction reaches to maximum conversion of toluene, the

reaction mixture was hot filtered and the filtrate was tested for presence of copper by AAS analysis. It ascertains the absence copper in the solution ruled out the possibility of any leaching during the catalyst recycle experiments. To draw further information the reused Cu@POP-Am2 was characterized by recording FTIR spectra and PXRD pattern (Figure 5.8).

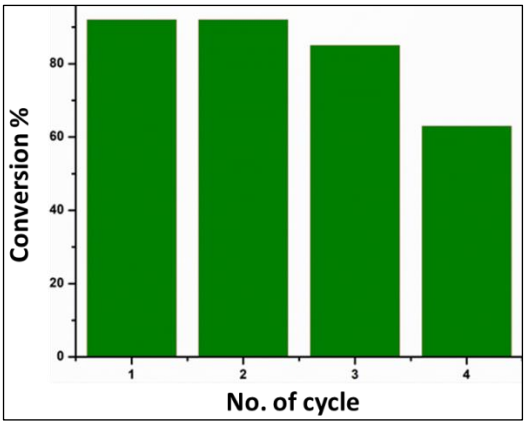

Figure 5.7 Conversion % of toluene vs no. of cycle revealing the reusable efficiency of Cu@POP-Am2.

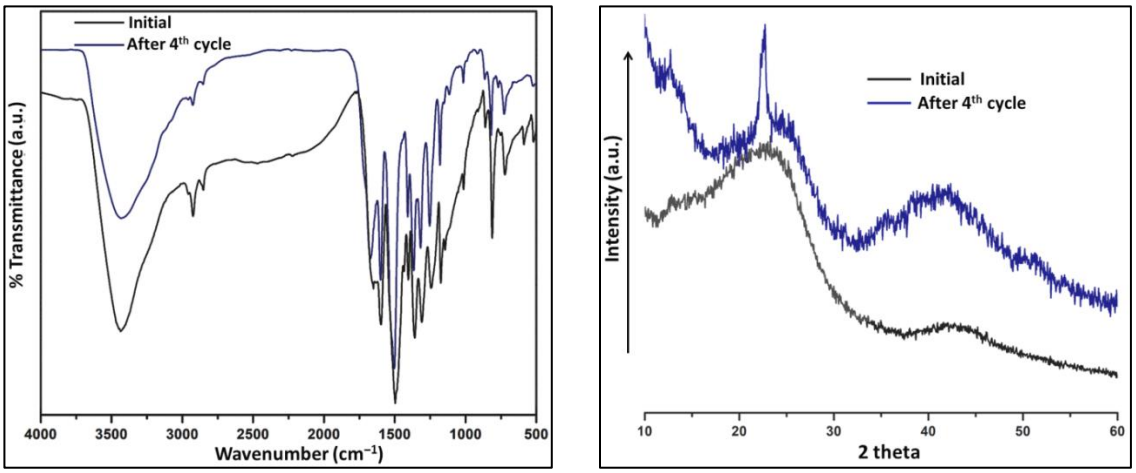

(a) (b)

Figure 5.8 Stacked IR spectra (a) and PXRD patterns (b) of fresh and reused Cu@POP-Am2 upto 4th catalytic cycle.

The IR spectrum of reused material is identical with that of the initial material thereby denying the possibility of Cu@POP-Am2 degradation. The PXRD pattern (Figure 5.8b) shows the appearance of sharp peak at 2θ = ~23° which was absent initially for the fresh unused Cu@POP-Am2. The possibility of transforming Cu into its oxidized form of $Cu(OH)_2$ by reacting with hydroxyl radical available in the reaction mixture could be reason of such intense peak at 2θ = ~23°. This peak of reused Cu@POP-Am2 closely

resembles to that of $Cu(OH)_2$ at 2θ angle ~24° [52]. Formation of copper hydroxide poisons the catalytic activity of Cu@POP-Am2 and thereby oxidative conversion of toluene decreases with increase in catalytic cycles.

5.3.5 Reaction mechanism study

Due to +I - effect of methyl group the benzylic carbon in toluene is electron deficient. Subsequently the sp^3 C–H σ-bond of methyl becomes weaker. It is speculated that in the reaction mixture toluene is stabilized at the metal surface of Cu@POP-Am2 via interaction of C–H bond. The Cu(II) in Cu@POP-Am2 is enriched in electron density by the donation of electrons from π-electron rich POP-Am2. Then the reverse charge transfer from filled metal dπ orbital to the antibonding σ* orbital of C–H bond takes place as the π-back donation from metal site is greater than σ-donation of C–H bond. Eventually it activates the weaker C–H bond to be broken (Step I, Scheme 5.4). Such activation ignited by the π-back donation of electrons is known as nucleophilic activation. In the subsequent step TBHP coordinates with the metal and simultaneously benzyl alcohol is formed (Step II, Scheme 5.4).

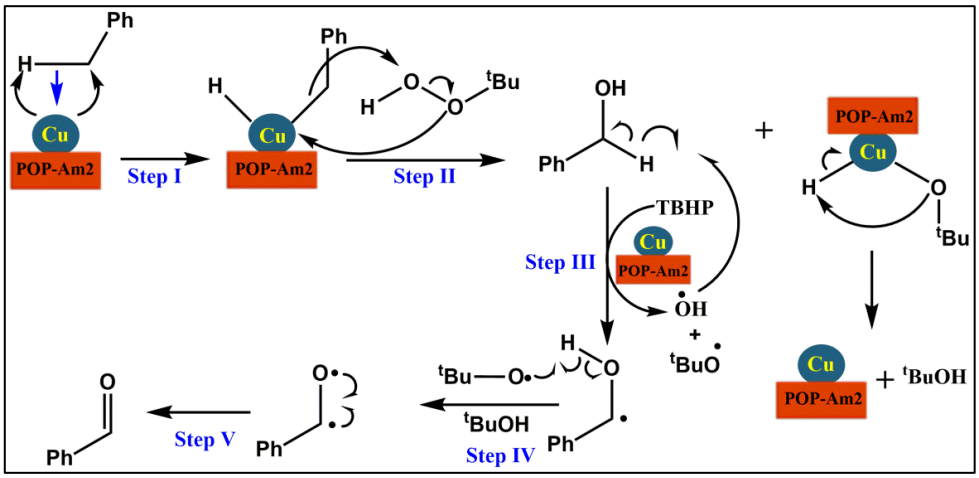

Scheme 5.4 Proposed mechanistic pathway of oxidation of toluene initiated via nucleophilic C–H activation by Cu@POP-Am2.

The intermediate benzyl alcohol thus formed reacts with hydroxyl radical that is generated from TBHP by Cu@POP-Am2 to yield hydroxyl benzyl radical (Step III, Scheme 5.4) that is stabilized by delocalization of free radical in the benzene ring and radical interactions with the catalyst surface. Following up, the *tert*-butoxy radical abstracts the hydroxyl proton of hydroxyl benzyl radical afforded benzaldehyde (Step

IV-V, Scheme 5.4). The benzaldehyde formed immediately stabilized at the catalyst surface via π···π and weak intermolecular interactions. This stabilization prevents the possibility of over oxidation. On the other hand, the *tert*-butoxide ion that coordinates with Cu(II) in step II (Scheme 5.4) further releases as *tert*-butanol and Cu@POP-Am2 is freed to undergo further catalytic reaction.

5.4 Summary

In this chapter, the electron rich POP that is discussed in Chapter 4, has been employed as support solid matrix to impregnate copper onto it (Cu@POP-Am2). Cu loaded POP-Am2 material was characterized by FTIR, PXRD, TGA, SEM, EDX and XPS analytical techniques. The copper metalation of the π-electrons rich carboxamide functionalized triazine ring based POP-Am2 affords an efficient, effective and inexpensive metal immobilized heterogeneous catalyst, tested successfully for the oxidation of benzylic C–H via nucleophilic activation. The Excellent catalytic activity in the nucleophilic activation and oxidation of sp^3 C–H of toluene and its derivative to afford benzaldehyde selectivity is emphasized. This study also provides an understanding in designing inexpensive copper catalyst supported on π-rich POP which paves the way towards direct functionalization of sp^3 C–H bonds.

5.5 Experimental Section

5.5.1 Materials

Triflic acid, 4-cyano aniline and 1,3,5-benzenetricarbonyl trichloride were brought from Alfa Aesar. Copper(II)acetate monohydrate, *tert*-butyl hydroperoxide, solvents of HPLC grade 1,4-dioxane and dichloromethane (DCM) were brought from MERCK. TEXM (T= toluene, E= ethylbenzene, X= xylenes, M= mesitylene) was obtained from Sigma Aldrich. All these chemicals have been used as received.

5.5.2 Synthesis of nitrogen POP-Am2

The nitrogen rich porous organic polymer has been synthesized from triazine ring based building unit 1,3,5-tris-(4-aminophenyl)triazine (TAPT) and trimesoyl chloride. The details of the synthetic procedure and the characterization of POP-Am2 have been discussed in chapter 4. The characterized POP-Am2 has been considered as scaffold for the impregnation of Cu(II) complex onto porous polymer.

5.5.3 Synthesis of copper impregnated POP-Am2 (Cu@POP-Am2)

A mixture of 50 mg of guest free POP-Am2 that has been synthesized and characterized in chapter 4 and copper acetate monohydrate (5 mg) was placed in 5 mL dichloromethane (DCM), stirred continuously for 24 h at room temperature. The solid reaction mixture was filtered, washed thoroughly with DCM, methanol, water and acetone ensuring the removal of non-adsorbed copper acetate. Thus obtained solid of Cu@POP-Am2 was further dried under vacuum desiccator and considered for further analysis.

5.5.4 FT-IR spectroscopy

FT-IR analyses have been carried out by recording the spectra in IR spectrophotometer made by Perkin Elmer in 400–4000 cm^{-1} frequency range. Ground 1 mg (approx) of the sample whose IR spectrum is to be recorded with about 100 mg of dry KBr and pressed the powdery mixture in order to obtain the suitable pellet by hydraulic pressure. Thus obtained pellet was considered for recording the IR spectrum.

5.5.5 Powder X–ray diffraction (PXRD) analysis

PXRD patterns were recorded on Bruker AXS (D8 FOCUS) using Cu Kα radiation with 2θ ranging from 5°–60° (step size 0.01°) at the rate of 1° min^{-1}. Initially the sample to be recorded has been vacuum dried ensuring it to be solvent free and ground about 50 mg of it to fine powder using mortar and pestle. Thus obtained fine powder was considered for recording the PXRD patterns.

5.5.6 Thermogravimetric analysis (TGA)

The thermal stability of a sample is reflected by performing the TGA analysis. The sample to be analyzed was initially dried under nitrogen environment, placed approximately 5 mg of it in platinum crucible and the analysis was performed at thermal analyzer made by Schimadzu under the constant flow of nitrogen at 10 °C min^{-1} heating rate.

5.5.7 BET surface area analysis

The analysis was performed in order to examine the porosity and rigidity of the material in the Brunauer– Emmett– Teller (BET) surface area analyzer made of Quantachrome Instruments (Ver 3.01). Prior to analysis the respective sample was degassed at 180 ºC

for 5 h and measured the N_2 adsorption-desorption isotherm for calculating the specific surface area, pore size and pore volume associated with the materials. The liquid nitrogen used in analysis was of ultra-high purity (99.999% pure) and the temperature during the entire process has been controlled by refrigerated bath of liquid nitrogen (77 K).

5.5.8 Electron microscopy analysis

The surface image of the bare MOP-Am2 and the Cu(II) impregnated MOP-Am2 (Cu@MOP-Am2 hereafter) have been captured by scanning electron microscope (SEM, JSM 6390) made by JEOL to examine the surface morphology. The electron dispersive X-ray spectrophotometer (EDS, JEOL) was employed to gather the presence of Cu in Cu@MOP-Am2. Data for both SEM and EDS experiment was collected at the accelerating voltage of 200 kV.

5.5.9 X-ray photoelectron spectroscopy (XPS) analysis

XPS study in order to examine the oxidation state of copper and its interaction site in POP-Am2 has been conducted with ESCALAB 220 XL spectrometer having monochromatic Al Kα X-ray source (1486.6 eV). The spherical energy analyzer has been operated in the constant analyzer energy (CAE) mode employing the electromagnetic lens mode. The angle between X-rays and the analyzer is fixed at 58° with the detection angle of photoelectrons at 30°.

5.6 References

[1] Blaser, H. U., Siegrist, U., Steiner, H., Studer, M., Sheldon, R. A. and van Bekkum, H. Fine chemicals through heterogeneous catalysis. *Wiley/VCH, Weinheim*, 389. 2001.

[2] Thomas, J. M., Raja, R., Sankar, G. and Bell, R. G. Molecular-sieve catalysts for the selective oxidation of linear alkanes by molecular oxygen. *Nature*, 398(6724):227, 1999.

[3] Stahl, S. S. Palladium oxidase catalysis: Selective oxidation of organic chemicals by direct dioxygen-coupled turnover. *Angewandte Chemie International Edition*, 43(26):3400-3420, 2004.

[4] Gaster, E., Kozuch, S. and Pappo, D. Selective aerobic oxidation of methylarenes to benzaldehydes catalyzed by N-hydroxyphthalimide and

cobalt(II) acetate in hexafluoropropan-2-ol. *Angewandte Chemie International Edition*, 56(21):5912-5915, 2017.

[5] Chen, M. S. and White, M. C. A predictably selective aliphatic C–H oxidation reaction for complex molecule synthesis. *Science*, 318(5851):783-787, 2007.

[6] Crabtree, R. H. and Lei, A. Introduction: C–H Activation. *Chemical Reviews*, 117(13):8481-8482, 2017.

[7] Dong, Z., Ren, Z., Thompson, S. J., Xu, Y. and Dong, G. Transition-metal-catalyzed c–h alkylation using alkenes. *Chemical Reviews*, 117(13):9333-9403, 2017.

[8] Ruiz-Castillo, P. and Buchwald, S. L. Applications of palladium-catalyzed C–N cross-coupling reactions. *Chemical Reviews*, 116(19):12564-12649, 2016.

[9] Wang, X., Li, N., Li, Z. and Rao, H. Copper-catalyzed dehydrogenative c(sp^2)–n bond formation via direct oxidative activation of an anilidic N–H bond: Synthesis of benzoimidazo [1,2-a] indoles. *The Journal of Organic Chemistry*, 82(19):10158-10166, 2017.

[10] Jayakumar, J., Parthasarathy, K. and Cheng, C. H., One-Pot Synthesis of isoquinolinium salts by rhodium-catalyzed C–H bond activation: Application to the total synthesis of oxychelerythrine. *Angewandte Chemie International Edition*, 124(1):201-204, 2012.

[11] Leow, D., Li, G., Mei, T. S. and Yu, J. Q. Activation of remote meta-C–H bonds assisted by an end-on template. *Nature*, 486(7404):518-522, 2012.

[12] Shen, P. X., Wang, X. C., Wang, P., Zhu, R. Y. and Yu, J. Q. Ligand-enabled meta-c–h alkylation and arylation using a modified norbornene. *Journal of the American Chemical Society*, 137(36):11574-11577, 2015.

[13] Xie, Y., Chen, T., Fu, S., Li, X. S., Deng, Y., Jiang, H. and Zeng, W. Pd-Catalyzed [3+2] cycloaddition of ketoimines with alkynes via directed sp^3 C–H bond activation. *Chemical Communications*, 50(73):10699-10702, 2014.

[14] Ye, J., Shi, Z., Sperger, T., Yasukawa, Y., Kingston, C., Schoenebeck, F. and Lautens, M. Remote C–H alkylation and C–C bond cleavage enabled by an in situ generated palladacycle. *Nature Chemistry*, 9(4):361-368, 2017.

[15] Xie, Y., Wu, X., Li, C., Wang, J., Li, J. and Liu, H., Ruthenium (II)-catalyzed redox-neutral [3+ 2] annulation of indoles with internal alkynes via C–H bond activation: accessing a pyrroloindolone scaffold. *The Journal of Organic Chemistry*, 82(10):5263-5273, 2017.

[16] Talukdar, D., Borah, S. and Chaudhuri, M. K. Bis(acetylacetonato)copper(II) catalyzed oxidative cross-dehydrogenative coupling (CDC) for the synthesis of α-acyloxy ethers through direct activation of α-C(sp^3)–H bond of cyclic ether. *Tetrahedron Letters*, 56(20):2555-2558, 2015.

[17] Pankhurst, J. R., Curcio, M., Sproules, S., Lloyd-Jones, G. C. and Love, J. B. Earth-abundant mixed-metal catalysts for hydrocarbon oxygenation. *Inorganic Chemistry*. 57(10):5915–5928, 2018.

[18] Annamalai, P., Hsu, K. C., Raju, S., Hsiao, H. C., Chou, C. W., Lin, G. Y., Hsieh, C. M., Chen, P. L., Liu, Y. H. and Chuang, S. C. Palladium(II)-catalyzed mono- and bis-alkenylation of n-acetyl-2-aminobiaryls through regioselective C-H bond activation. *The Journal of Organic Chemistry*, 83(7):3840-3856, 2018.

[19] Wang, X. C., Gong, W., Fang, L. Z., Zhu, R. Y., Li, S., Engle, K. M. and Yu, J. Q. Ligand-enabled meta-C–H activation using a transient mediator. *Nature*, 519(7543):334-338, 2015.

[20] Smalley, A. P. and Gaunt, M. J. Mechanistic Insights into the palladium-catalyzed aziridination of aliphatic amines by C–H activation. *Journal of the American Chemical Society*, 137(33):10632-10641, 2015.

[21] Gandeepan, P. and Cheng, C. H. Transition-metal-catalyzed π-bond-assisted C–H bond functionalization: An emerging trend in organic synthesis. *Chemistry–An Asian Journal*, 10(4):824-838, 2015.

[22] Pascanu, V., Carson, F., Solano, M. V., Su, J., Zou, X., Johansson, M. J. and Martín-Matute, B. Selective heterogeneous C–H activation/halogenation reactions catalyzed by Pd@MOF nanocomposites. *Chemistry-A European Journal*, 22(11):3729-3737, 2016.

[23] Wang, Z. J., Lv, J. J., Yi, R. N., Xiao, M., Feng, J. J., Liang, Z. W., Wang, A. J. and Xu, X. Nondirecting group sp^3 C−H activation for synthesis of bibenzyls via homo-coupling as catalyzed by reduced graphene oxide supported PtPd@Pt porous nanospheres. *Advanced Synthesis & Catalysis*, 360(5):932-941, 2018.

[24] Sosa, V., Melkie, M., Sulca, C., Li, J., Tang, L., Li, J., Faris, J., Foley, B., Banh, T., Kato, M. and Cheruzel, L. E. Selective light-driven chemoenzymatic trifluoromethylation/hydroxylation of substituted arenes. *ACS Catalysis*, 8(3):2225-2229, 2018.

[25] Zeng, L., Li, H., Tang, S., Gao, X., Deng, Y., Zhang, G., Pao, C. W., Chen, J. L., Lee, J. F. and Lei, A. Cobalt-catalyzed electrochemical oxidative C–H/N–H carbonylation with hydrogen evolution. *ACS Catalysis*. 8:5448-5453, 2018.

[26] Luo, Y., Ma, Y. and Hou, Z. α-C—H Alkylation of methyl sulfides with alkenes by a scandium catalyst. *Journal of the American Chemical Society*. 140(1):114-117, 2018.

[27] Chen, C., Xu, X. H., Yang, B. and Qing, F. L. Copper-catalyzed direct trifluoromethylthiolation of benzylic C–H Bonds via nondirected oxidative C(sp^3)–H Activation. *Organic Letters*, 16(12):3372-3375, 2014.

[28] Yu, H., Li, Z. and Bolm, C. Nondirected copper-catalyzed sulfoxidations of benzylic C–H bonds. *Organic Letters*, 20(7):2076-2079, 2018.

[29] Marcoux, J. F., Doye, S. and Buchwald, S. L. A general copper-catalyzed synthesis of diaryl ethers. *Journal of the American Chemical Society*, 119(43):10539-10540, 1997.

[30] Zanon, J., Klapars, A. and Buchwald, S. L. Copper-catalyzed domino halide exchange-cyanation of aryl bromides. *Journal of the American chemical Society*, 125(10):2890-2891, 2003.

[31] Jerphagnon, T., Van Klink, G. P., de Vries, J. G. and van Koten, G. Aminoarenethiolate-Copper(I)-catalyzed amination of aryl bromides. *Organic Letters*, 7(23):5241-5244, 2005.

[32] Fei, H. and Cohen, S. M. Metalation of a thiocatechol-functionalized Zr(IV)-based metal−organic framework for selective C−H functionalization. *Journal of the American Chemical Society*, 137(6):2191-2194, 2015.

[33] Qin, Y., Zhu, L. and Luo, S. Organocatalysis in inert C–H bond functionalization. *Chemical Reviews*, 117(13):9433-9520, 2017.

[34] Kesavan, L., Tiruvalam, R., Ab Rahim, M. H., bin Saiman, M. I., Enache, D. I., Jenkins, R. L., Dimitratos, N., Lopez-Sanchez, J. A., Taylor, S. H., Knight, D. W. and Kiely, C. J. Solvent-free oxidation of primary carbon-hydrogen bonds in toluene using Au-Pd alloy nanoparticles. *Science*, 331(6014):195-199, 2011.

[35] Bruhne F. and Wright, E. Ullmann's encyclopedia of industrial chemistry, *Wiley-VCH, Weinheim*, 5:223, 2012.

[36] Partenheimer, W., The high yield synthesis of benzaldehydes from benzylic alcohols using homogeneously catalyzed aerobic oxidation in acetic acid. *Advanced Synthesis & Catalysis*, 348(4-5):559-568, 2006.

[37] Yuan, H., Fang, X., Ma, Q., Mao, J., Chen, K., Chen, Z. and Li, H., New mechanistic insight into the aerobic oxidation of methylaromatic compounds catalyzed by Co–Mn–Br and its applications. *Journal of Catalysis*, 339:284-291, 2016.

[38] Partenheimer, W. Methodology and scope of metal/bromide autoxidation of hydrocarbons. *Catalysis Today*, 23(2):69-158, 1995.

[39] Wang, Y., Li, H., Yao, J., Wang, X. and Antonietti, M. Synthesis of boron doped polymeric carbon nitride solids and their use as metal-free catalysts for aliphatic C–H bond oxidation. *Chemical Science*, 2(3):446-450, 2011.

[40] Li, X. H., Wang, X. and Antonietti, M. Solvent-free and metal-free oxidation of toluene using O_2 and g-C_3N_4 with nanopores: nanostructure boosts the catalytic selectivity. *ACS Catalysis*, 2(10):2082-2086, 2012.

[41] Zhang, Y., Zhao, Y., Luo, Y., Xiao, L., Huang, Y., Li, X., Peng, Q., Liu, Y., Yang, B., Zhu, C. and Zhou, X. Directed aromatic C–H activation/acetoxylation catalyzed by Pd nanoparticles supported on graphene oxide. *Organic Letters*, 19(24):6470-6473, 2017.

[42] Modak, A., Mondal, J. and Bhaumik, A. Highly porous organic polymer containing free -CO_2H groups: A convenient carbocatalyst for indole C–H activation at room temperature. *ChemCatChem*, 5(7):1749-1753, 2013.

[43] Yang, Q. Y., Lama, P., Sen, S., Lusi, M., Chen, K. J., Gao, W. Y., Shivanna, M., Pham, T., Hosono, N., Kusaka, S., Perry IV, J. J., Ma, S., Space, B., Barbour, L. J., Kitagawa, S. and Zaworotko, M. J. Reversible switching between highly porous and nonporous phases of an interpenetrated diamondoid coordination network that exhibits gate-opening at methane storage pressures. *Angewandte Chemie International Edition*. 57(20):5684-5689, 2018.

[44] Patil, R. S., Banerjee, D., Simon, C. M., Atwood, J. L. and Thallapally, P. K. Noria: A highly Xe-selective nanoporous organic solid. *Chemistry-A European Journal*, 22(36):12618-12623, 2016.

[45] Gupta, S. K., Kaleeswaran, D., Nandi, S., Vaidhyanathan, R. and Murugavel, R. Bulky isopropyl group loaded tetraaryl pyrene based azo-linked covalent

organic polymer for nitroaromatics sensing and CO_2 adsorption. *ACS Omega*, 2(7):3572-3582, 2017.

[46] Ma, D., Li, B., Cui, Z., Liu, K., Chen, C., Li, G., Hua, J., Ma, B., Shi, Z. and Feng, S. Multifunctional luminescent porous organic polymer for selectively detecting iron ions and 1,4-dioxane via luminescent turn-off and turn-on sensing. *ACS Applied Materials & Interfaces*, 8(36):24097-24103, 2016.

[47] Samanta, P., Desai, A. V., Anothumakkool, B., Shirolkar, M. M., Karmakar, A., Kurungot, S. and Ghosh, S. K. Enhanced proton conduction by post-synthetic covalent modification in a porous covalent framework. *Journal of Materials Chemistry A*, 5(26):13659-13664, 2017.

[48] Kang, D. W., Song, J. H., Lee, K. J., Lee, H. G., Kim, J. E., Lee, H. Y., Kim, J. Y. and Hong, C. S. A conductive porous organic polymer with superprotonic conductivity of a Nafion-type electrolyte. *Journal of Materials Chemistry A*, 5(33):17492-17498, 2017.

[49] Khatioda, R., Talukdar, D., Saikia, B., Bania, K. K. and Sarma, B. Constructing two dimensional amide porous polymer to promote selective oxidation reactions. *Catalysis Science & Technology*, 7(14):3143-3150, 2017.

[50] Khatioda, R., Pathak, D. and Sarma, B. Cu (II) Complex onto a pyridine-based porous organic polymer as a heterogeneous catalyst for nitroarene reduction. *ChemistrySelect*, 3(23):6309-6320, 2018.

[51] Singuru, R., Dhanalaxmi, K., Shit, S. C., Reddy, B. M. and Mondal, J. Palladium nanoparticles encaged in a nitrogen-rich porous organic polymer: Constructing a promising robust nanoarchitecture for catalytic biofuel upgrading. *ChemCatChem*, 9(13):2550-2564, 2017.

[52] Li, Z., Xin, Y., Zhang, Z., Wu, H. and Wang, P. Rational design of binder-free noble metal/metal oxide arrays with nanocauliflower structure for wide linear range nonenzymatic glucose detection. *Scientific Reports*, 5:10617, 2015.